Reducing Noise Caused by Tilt-to-Length Coupling in Simulated LISA Data

Skylar A. Kemper
kempers@my.erau.edu

Mentors:

Dr. Roberta Giusteri, Dr. Sarah Paczkowski, Dr. Gudrun Wanner, and Megha Dave

Funded by the University of Florida, Gainseville, USA
NSF Grant Numbers : PHY-1950830 and NSF PHY-1460803
Research Collaboration with the Albert Einstein Institute, Hannover, Germany

Contents

1 Abstract

Angular instability in the LISA satellites leads to a unique noise known as Tilt-to-Length Coupling (TTL). This paper explores two methods for reducing the noise created by TTL. The first half of the paper explores Geometric TTL estimations, because Geometric TTL is effected by the design of the test mass interferometers and long arm interferometers, the first goal was to identify where TTL impacts results significantly by creating estimations for beam waist changes and photodiode shifts. The second half of the paper explores methods for subtracting TTL noise from a simulated data set with Galactic Foreground Noise injected into it. For Geometric TTL estimations, We were able to achieve TTL estimations below desired noise range (10^{-12}) around an average 10^{-13}. In regards to the TTL subtraction, we found that Foreground noise makes a difference in the TTL coefficient results, and we achieved better estimations for TTL coefficients when adjusting the frequency range from 1e-4 (Hz) to 2e-3 (Hz). However, we were unable to achieve a range capable of subtracting TTL enough to be useful.

2 Introduction

The Laser Interferometer Space Antenna (LISA) is a project led by the European Space Agency (ESA) set to launch in the early 2030's [4]. LISA is following the successful detection of gravitational waves using ground based interferometers. Gravitational waves have allowed us to observe the universe at a deeper level, such as when the LIGO detectors' were able to record gravitational waves caused by a pair of black holes merging in 2015[3]. Additionally, LISA also follows several space interferometers, such as LISA Pathfinder, which provided insight into how a space based interferometry system can

function. Lisa Pathfinder utilized specialized inertial sensors, a drag-free control system, micro-propulsion, and a laser metrology system. Considering LISA Pathfinder used many of the same technologies intended for LISA, it allowed physicists to observe noise and errors which LISA will encounter and figure out solutions before LISA launches [2]. A space-based interferometer will provide a reduction in seismic and gravity gradient noise that would have interfered with low frequency observations on earth. LISA consists of three identical spacecraft moving in orbit, behind the Earth. The duration of the project will span 4-years and LISA will be capable of detecting Black Hole binaries, Compact binaries, Extreme Mass Ratio Inspirals, and other bodies with gravitational waves between 0.1mHz and 100mHz [1].

3 Theory

LISA Pathfinder observed the impact of Tilt-To-Length (TTL) noise interfering with its results after it's launch. The TTL presented itself as a bulge between the 200mHz - 20 mHz frequency range. This is produced by the effects of cross coupling the jitters of the satellite into the longitudinal readout, see figure (1). TTL noise is specific to the current design being used for space interferometry because of the test mass and long arm interferometers.

The current LISA set-up includes three separate satellites with long arm interferometers exchanging beams of light between the free-falling test masses inside them. The distance between these satellites can be changed by gravitational waves. The test mass interferometers are used to measure the changes impacting the free-falling tests masses and the long arm interferometers between spacecraft. The satellites all have separate optical benches with the test mass interferometers to measure the distance changes for the

test mass inside that specific spacecraft and the optical bench itself. Meanwhile, the long arm interferometers measure changes which occur between the satellites locally and remotely. This makes for 6 test masses, 2 for each satellite, 6 test mass interferometers, and 3 long arm interferometers, all working in sync between spacecraft to detect gravitational waves based on changes in the interferometer's light path. LISA Pathfinder was able to demonstrate this concept on a single satellite, with only the test mass interferometers, leading to the problem with TTL [5].

Due to the impact of TTL on LISA Pathfinder's results the data was less useful. In order to remove the TTL noise, the subtraction method was applied. This method is accomplished by figuring out the coefficients for each of the jittering components and subtracting it from the frequency. The equation used for subtraction is depicted below and each component is the differential acceleration measurement for each jitter direction (1).

$$\Delta g_{x-talk} = C_1\ddot{\phi}[t] + C_2\ddot{\eta}[t] + C_3\ddot{y}[t] + C_4\ddot{\bar{z}}[t] + C_5\bar{y}[t] + C_6\bar{z}[t] + \delta_{ifo}\ddot{x}_1[t] \tag{1}$$

Figure (1) shows the LISA Pathfinder results with the jitter as well as the results with the jitter subtracted via equation (1).

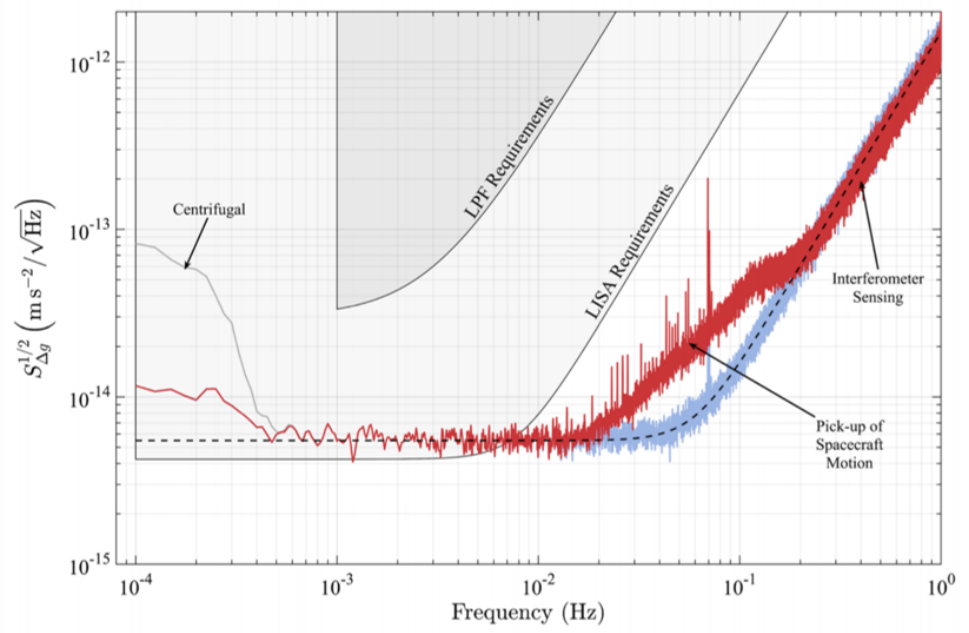

Figure 1: TTL Noise observed by LISA pathfinder is depicted in figure (1). The red curve includes noise caused by jitters in the satellite. The blue line shows the subtraction method being applied to the signal to reduce the geometric TTL. [6]

3.1 Geometric TTL Estimations

Geometric cross coupling is caused by lateral and angular jitters or movement in the spacecraft. Due to the free-falling masses moving with all degrees of freedom, the changes to the spacecraft cause lateral and angular movements in the test mass, which then changes the distance the beam of light travels after interacting with the test masses. Because LISA interferometer detections depend on changes to the length of light caused by gravitational waves, changing the path length through other sources disrupts results creating the noise. Therefore, TTL creates noise which can impact the results and confuse the actual signal [6].

For the Geometric TTL estimations, several aspects of geometric set up were considered. The Longitudinal Pathlength Signal (LPS) is the total distance the light travels throughout the simulation. The Optical Pathlength Difference (OPD) however, only refers to the change between the measurement beam (Mbeam) and the reference beam (Rbeam) caused by TTL. See equation (2).

$$OPD = Measurement\ \ Beam\ -\ Reference\ \ Beam \tag{2}$$

While the OPD and LPS refer to geometric components of the set-up, the non-geometric coefficient can be found by subtracting the LPS coefficient from the OPD coefficient.

$$Non-Geometric\ \ Component = LPS\ \ Coefficient\ -\ OPD\ \ Coefficient \tag{3}$$

The simulation used to estimate TTL was created using C++ and the IfoCAD software at the Albert Einstein Institute, it was designed as depicted in figure (2). The simulation includes a Quadrant Photodiode (QPD) to transition the light into voltage and read the signal for the amount of light (photons) present. There are two beams depicted in the set up, both beams are astigmatic gaussian beams which means they are elliptical instead of strictly circular. The measurement beam is the actual beam being observed, and it is a part of the LPS. The reference beam shows where the measurement beam is theoretically supposed to be, and it shows where we want the beam to be located.

The secondary factors to consider, which are depicted in figure (2), are the geometric changes simulated in the code which are observed throughout this project. Some of the

those observed changes include lateral and longitudinal shifts which are depicted by the green arrows. Outside of lateral and longitudinal shifts, we also observed changes to the measurement beams waist size and waist location, see figure (3).

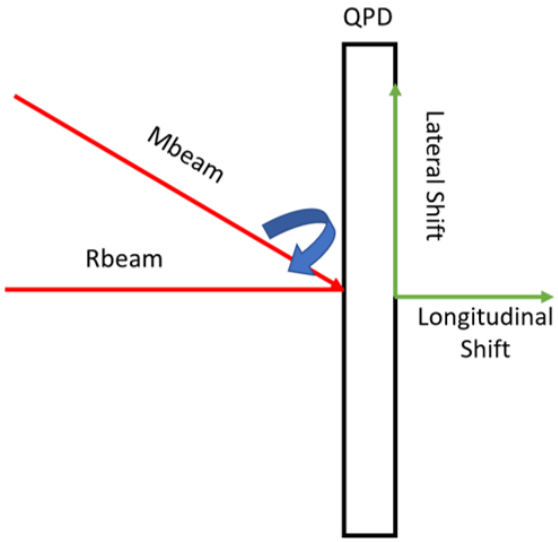

Figure 2: Diagram depicting the IfoCAD simulation in terms of what is theoretically happening if the simulation were real light beams and equipment.

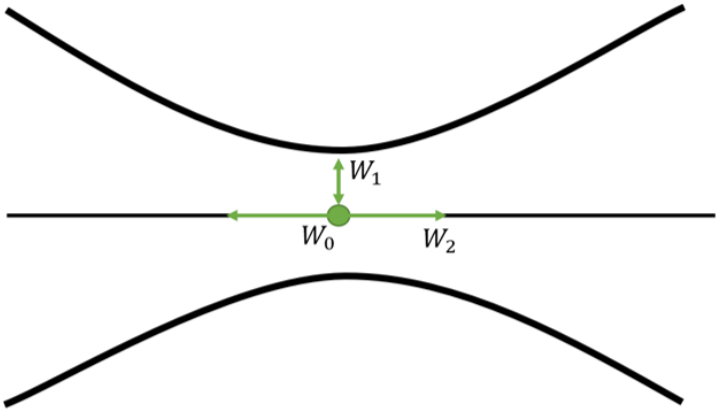

Figure 3: Diagram depicting the changes impacting the measurement beam waist for the IfoCAD simulation. Where the beam waist itself is defined by W_0, the changes to the beam waist size are represented by W_1 showing the squeezing and expanding of the beam waist. W_2 shows the beam waist location changes, where the beam waist W_0 is moved along the axis, changing the measurement beam divergence and shape.

The equation used to determine the TTL estimations is derived through creating graphs of the results. To begin, the first graph depicts the relationship between LPS offset (m) and the angle of the offset (rad). The data is fit to a second order polynomial as depicted by equation (4). Or a first order polynomial as depicted in equation (5).

$$LPS = C\frac{m}{rad^2}\phi^2 \tag{4}$$

$$LPS = C\frac{m}{rad}\phi \tag{5}$$

Next, a second graph is created using the Coefficient (C) ($\frac{m}{rad^2}$) values from the first

graph and equations (4) - (5). This graph depicts the Longitudinal or Lateral Offset of QPD (m) from the Coefficient value ($\frac{m}{rad^2}$). The second graph is used to find the value for the final Coefficient (Coeff.) ($\frac{\frac{m}{rad^2}}{m}$) using equation (6).

$$Coeff \ = \ C(1,1) * dlong + C(1,2) \tag{6}$$

Where dlong ($\frac{rad}{rtHz}$) represent the displacement longitudinal or lateral from the QPD. Using the values from equation (6), equation (7) can be created to find a TTL estimation.

$$TTL \ Estimation \ = \ 2 * Coeff * \phi * \phi_{off} \tag{7}$$

Where ϕ_{off} is the offset of the angle (ϕ) (rad) given in equation (8) for the data being analyzed.

$$\phi_{off} = 50 * 10^{-6} \tag{8}$$

The final equation used to determine the TTL estimation comes from combining equations (5) and (6) to create equation (9). The intercept comes from the intercept of each line from the secondary graphs (2).

$$TTL_{Estimation} \ = \ 2 * \phi_{off} * \phi * Coeff * dlong + Intercept \tag{9}$$

3.2 Tilt-to-Length Subtraction through Time Delay Interferometry

There are two central types of noises which impact LISA, Instrumental noise and Galactic Foreground Noise. Galactic Foreground Noise is composed of all the signals LISA will

measure from the galaxy. A majority of the noise comes from double white dwarf binaries which is why a lot of the time other sources are ignored in favor of just the white dwarf binaries. After a source has been identified, however, it can be subtracted from the overall Galactic Foreground Noise which allows us to whittle it down to just what can be resolved. The residual is what composes the the background noise.

For this project the Galactic Foreground noise is simulated using a LISAsolve software in which every binary is modeled in the frequency domain and only double binary white dwarfs are simulated. Unresolved Galactic Foreground Noise comes from subtracting resolved binary sources from the simulated population of binaries, creating the noise used in this project.

4 Results

4.1 Geometric TTL Estimations

Through running the simulation described under Geometric TTL estimation's theory section, without changing any variables, we were able to develop a graph for the angle and the LPS with a rotation at the photodiode center. However, in order to observe the impacts of longitudinal and lateral QPD shifts we added those shifts on to two separate graphs to observe the changes, see figures (4) and (5) respectively.

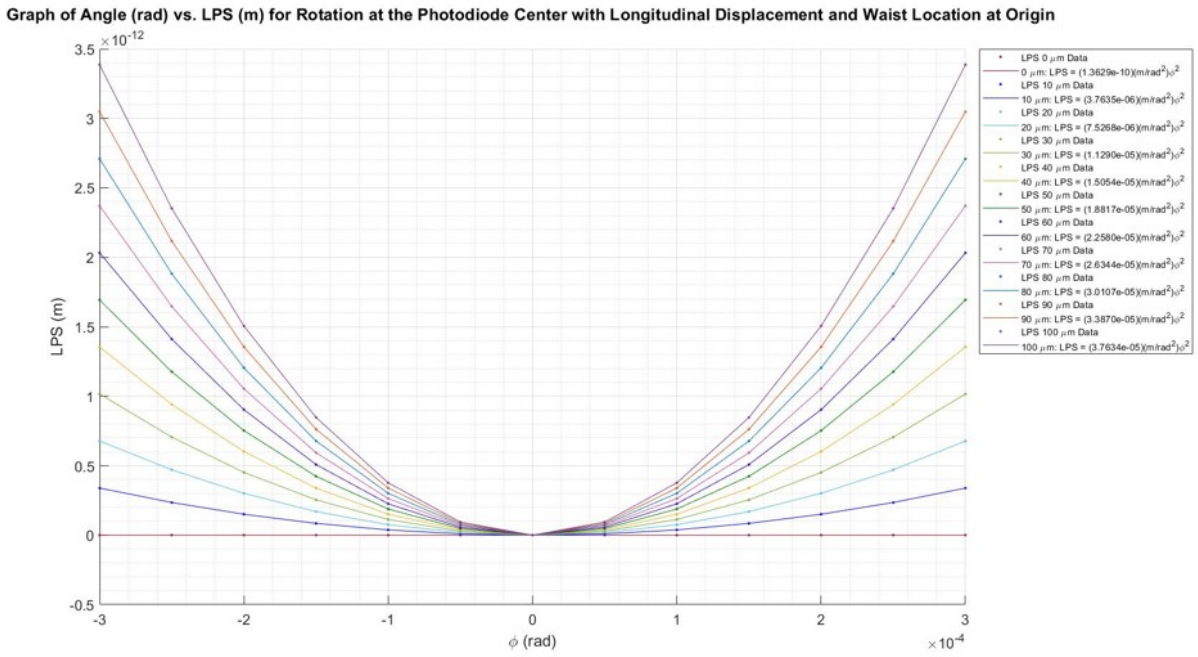

Figure 4: Graph depicting the angle (ϕ) vs the LPS(m) with longitudinal displacement in steps of 10µm from 0 to 100µm.

The impacts show a linear increase between each of the steps for both lateral and longitudinal displacement. Through using the coefficients for the slopes of each line we created another graph with the coefficients and the longitudinal shifts. This models the linear relationship between the steps. We repeated the process for the 4 beam waist location shifts, -1.5m, -.75m, .75m, and 1.5m. These shifts are chosen arbitrarily and are just to see a range of what is there. The process is repeated in the same manner, including the longitudinal and lateral shifts, but the measurement beam waist is shifted to -1.5m, -.75m, .75m, or 1.5m, respectively. For longitudinal shifts we get figure (5) and lateral shifts figure (6).

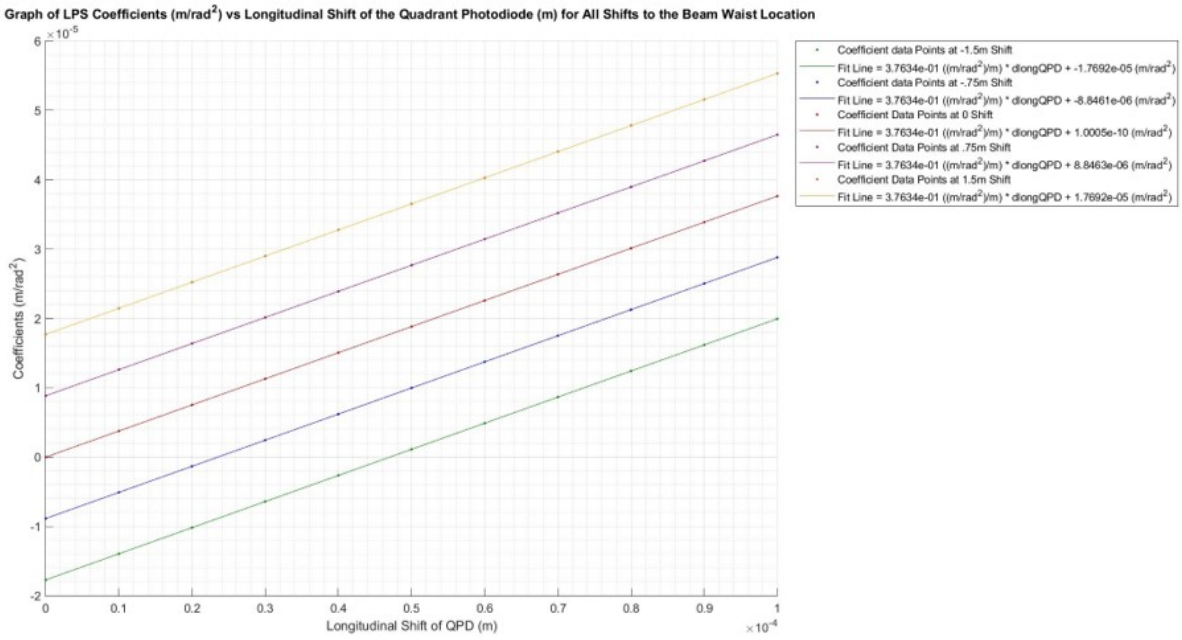

Figure 5: Graph depicting the QPD longitudinal offset (m) and the coefficients (C) (found using equation (4)) from the previous graphs for all 5 measurement beam waist location changes.

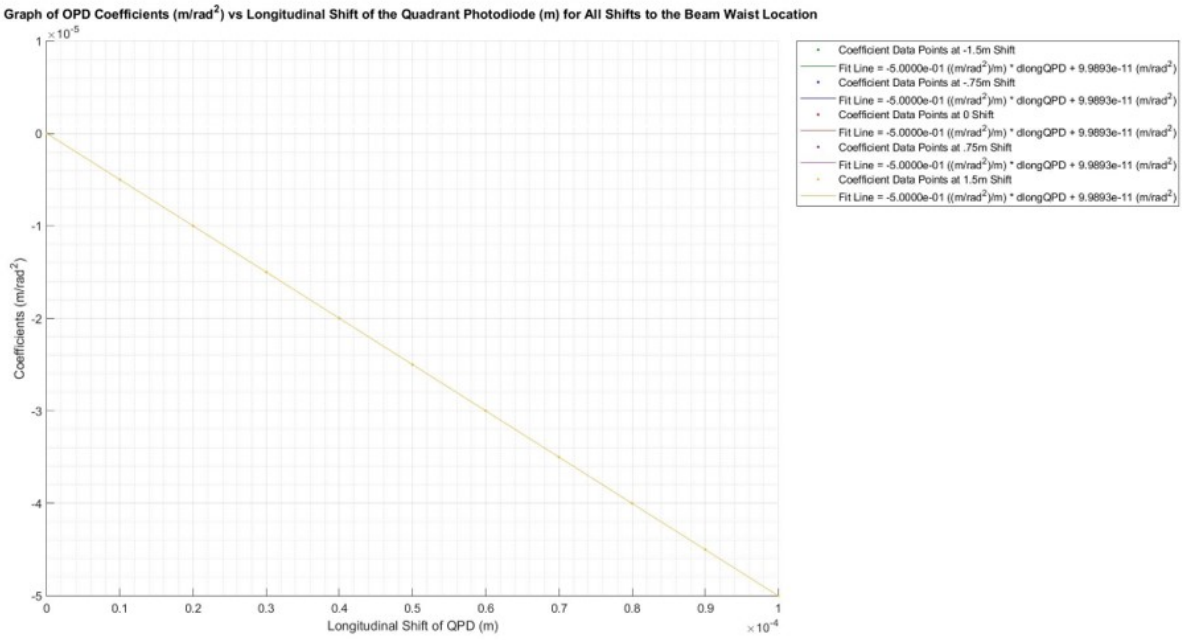

Figure 6: Graph depicting the lateral displacement (m) and the coefficients (C) (found using equation (5)) from the previous graphs for all 5 measurement beam waist location changes.

While the longitudinal displacements shown in figure (5) are impacted by the measurement beam waist location changes, the lateral displacement in figure (6) is not. This was also done for the OPD, but there were no significant changes made from the initial. Because there were no changes, the OPD data sets were not considered further. The fit line equations created from the secondary grouping of graphs with longitudinal or lateral offset of QPD (m) against the Coefficient values ($\frac{m}{rad^2}$) were used to find TTL estimations using equation (9).

The process was repeated for longitudinal and lateral data, however, instead of the beam waist location being shifted it was resized by factors of $5\%, 10\%, 0\%, -5\%, -10\%$ which equate to .0448m, .0224m, 0, -0.224m, .0448m. When applied to the normal beam

waist of 0.448m, the new beam waists are .4928, .4704m, .448m, .4256m, and .4032m. The first set of graphs is not depicted for the beam waist being resized. The secondary group of graphs for the coefficient and the LPS QPD shifts are depicted by figures (7) and (8) respectively.

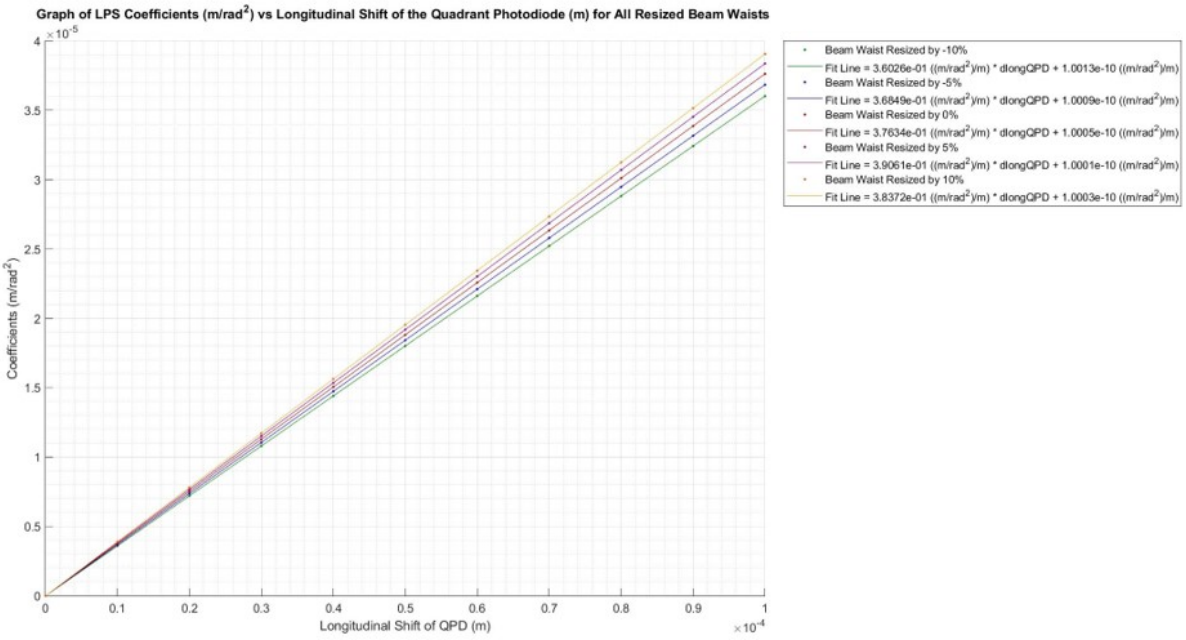

Figure 7: Graph depicting the longitudinal displacement (m) and the coefficients (C) (found using equation (4)) from the previous graphs for all 5 measurement beam waist resized.

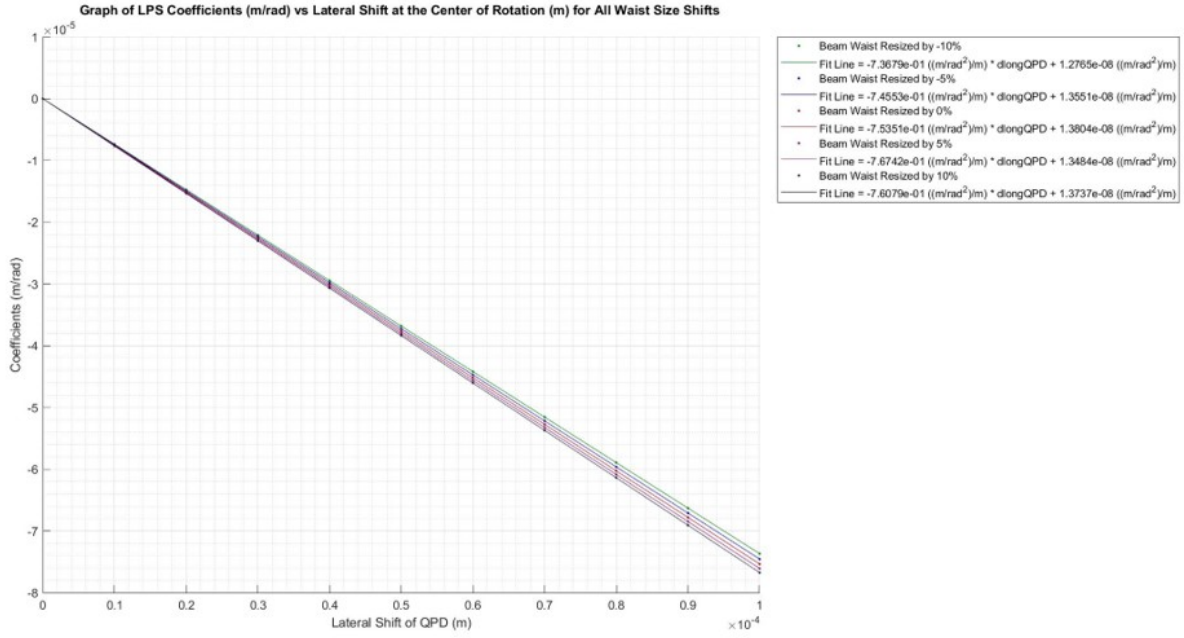

Figure 8: Graph depicting the lateral displacement (m) and the coefficients (C) (found using equation (5)) from the previous graphs for all 5 measurement beam waist resized.

The results for TTL estimations can be found in the conclusions section.

4.2 Tilt-to-Length Subtraction through Time Delay Interferometry

To begin the TTL subtraction project, the code had already been written to produce a graph of the Frequency (Hz) and the Amplitude Spectral Density ($mHz^{-\frac{1}{2}}$). Depicted for the Unlocked LISA configuration on Day 1 of recording the Foreground seen in figure (9). Where the red line represents the analytic TDI (Time Delay Interferometry), the green line shows the TDI X without Foreground noise, the black line shows the TDI X with Foreground noise, the cyan line is an artificial TTL contribution (2.3 (mm/rad)) pro-

grammed into the code which we are trying to estimate, and the magenta line represents TDI X with Foreground noise and TTL noise subtracted.

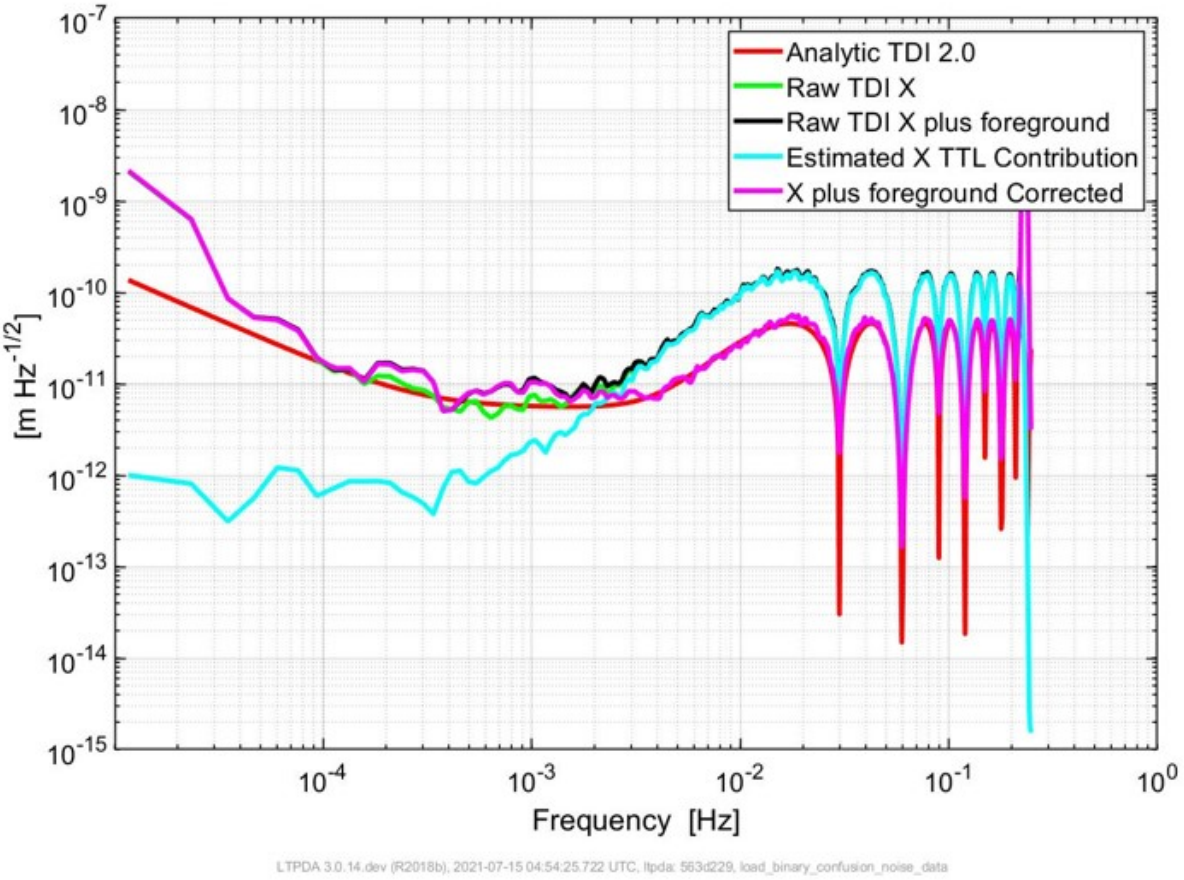

Figure 9: Graph of Frequency (Hz) vs. the Amplitude Spectral Density ($mHz^{-\frac{1}{2}}$) for Day 1 of the Unlocked LISA configuration.

A significant note in regards to figure (9) is that most of the variance occurs between 1e-4 (Hz) and 2e-3 (Hz). Because of this we later on extended the frequency from the 1e-4 (Hz) to 2e-3 (Hz). We created graphs of the Frequency (Hz) vs. the Amplitude Spectral Density ($mHz^{-\frac{1}{2}}$) for Days 1 - 5 of the Foreground data and LISA Configurations from

Unlocked, N1a, N2a, N1b, N2b, N1c, and N2c. In order to observe the changes caused by the Configurations, figure (10) was created. Figure (10) shows the Configurations against the Deviations for every variable of the TTL contributions which we are trying to estimate.

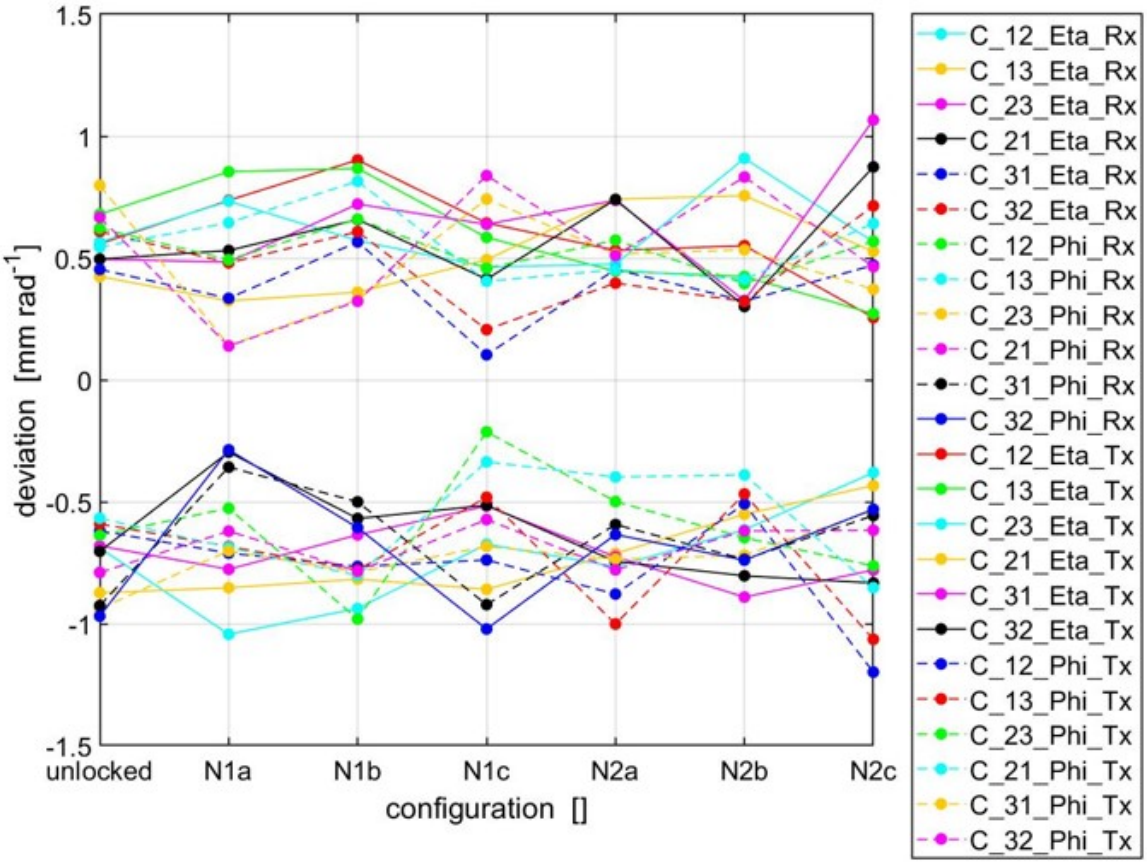

Figure 10: Graph of the Configurations vs the Deviations from each other for Day 1 of the Foreground data set.

We then repeated the same process for the days 1-5 showing Configuration Unlocked, represented in figure (11).

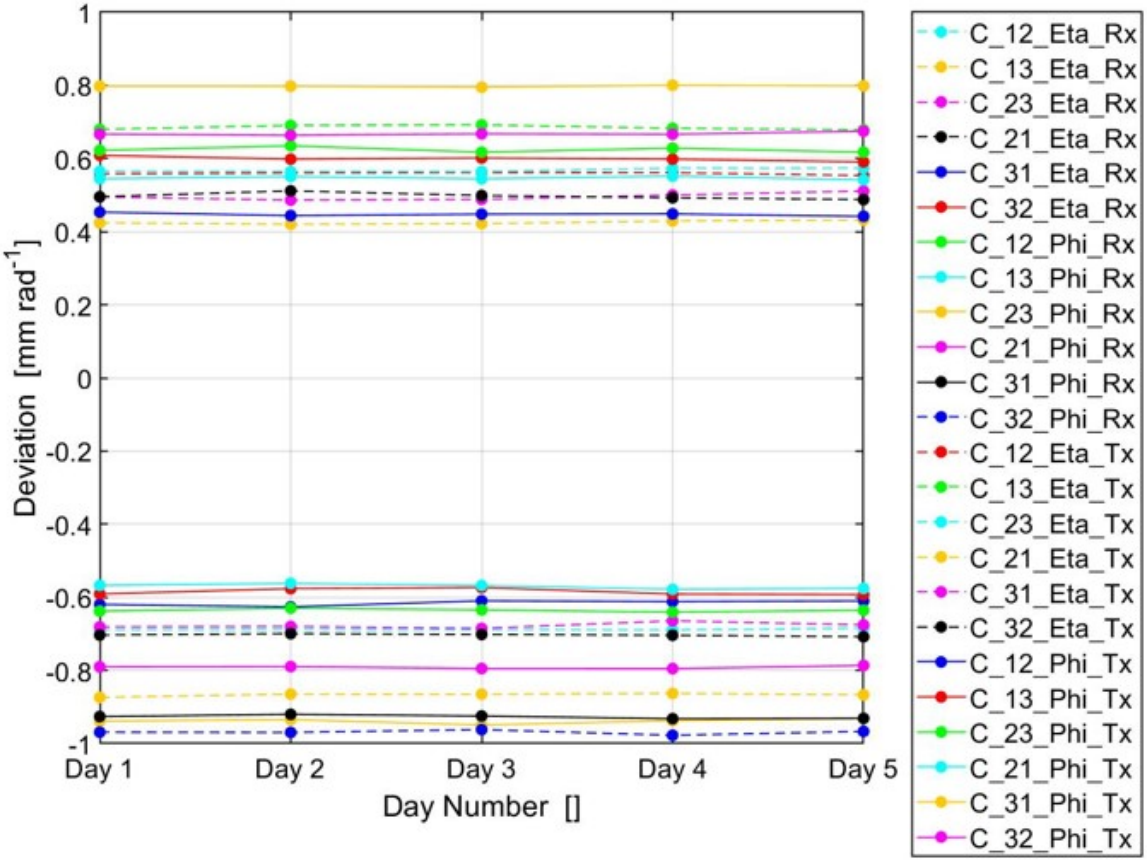

Figure 11: Graph of the Days vs the Deviations from each other for Configuration Unlocked of the Foreground data set.

Figures (10) and (11) show significant changes between the Configurations but otherwise linearity for the days of observation.

As explained beforehand, we then decided to observe the impact on the data when changing the frequency range from 1e-4 (Hz) to 2e-3 (Hz), resulting in figure (12).

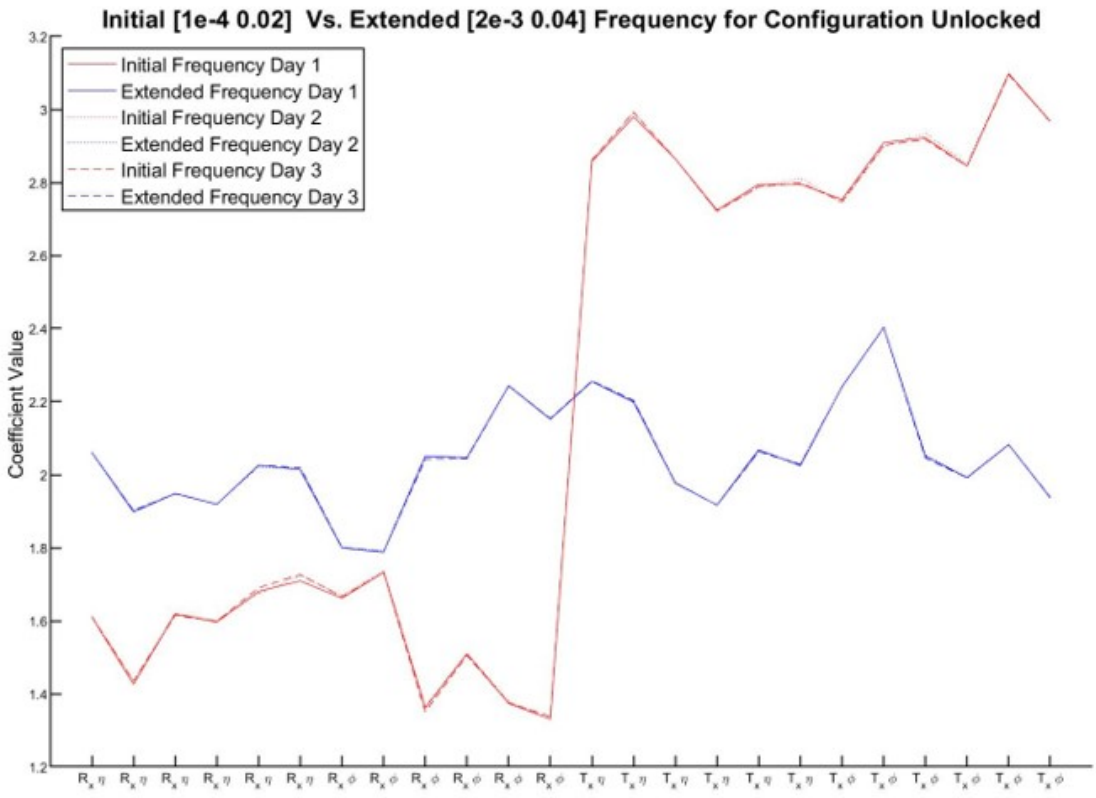

Figure 12: Graph of the coefficient value comparing the results with the initial frequency of 1e-4 (Hz) to the extended frequency of 2e-3 (Hz) for Unlocked data Configuration.

Considering the coefficients are set to 2.3 (mm/rad) as described earlier on in the paper, the extended frequency of 2e-3 (Hz) produces better results compared to the initial frequency of 1e-4 (Hz).

Figure (13) is the same as figure (12), but without the Foreground data, in order to observe the frequency initial vs. extended impact on the results. Figure (13) shows the coefficient guesses are closer with the extended frequency of 2e-3 (Hz).

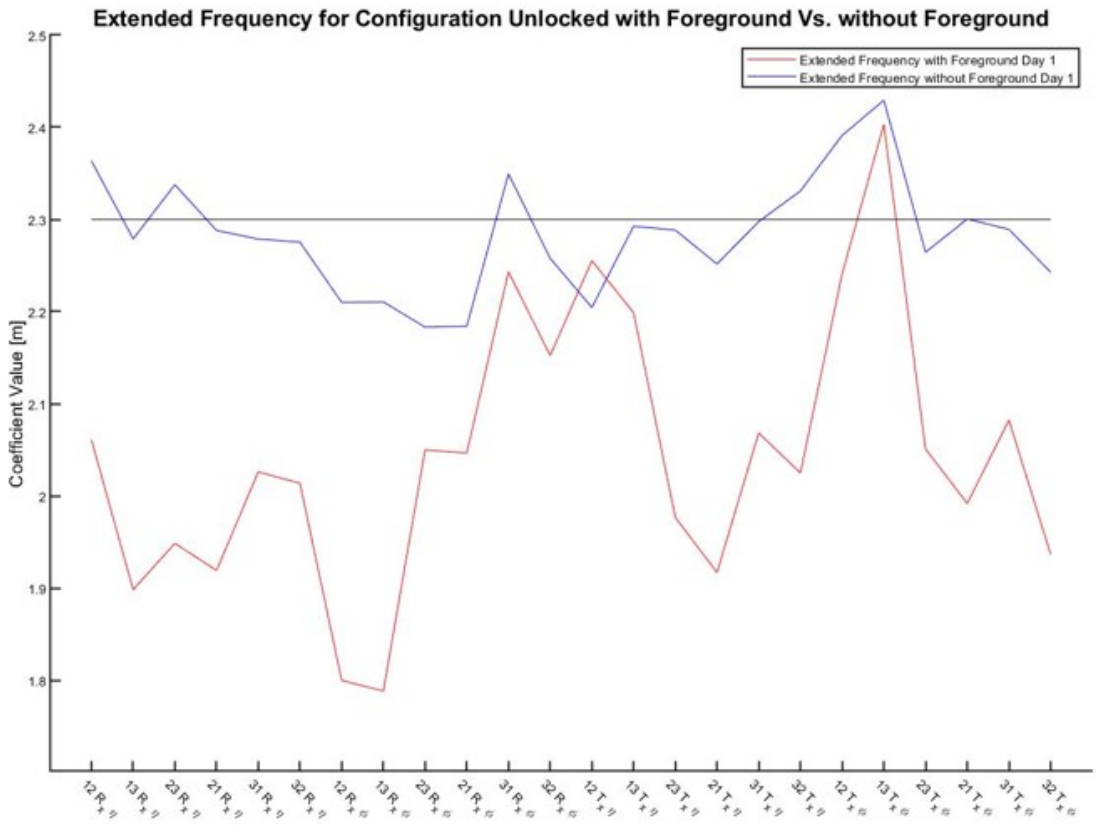

Figure 13: Graph of the coefficient value comparing the results with the initial frequency of 1e-4 (Hz) to the extended frequency of 2e-3 (Hz) without Foreground noise using the Unlocked Configuration.

5 Conclusion

5.1 Geometric TTL Estimations

Using the derivation found between pages (8) and (9), equation (9) is used to determine the TTL Estimations using data from the secondary grouping of graphs.

The first table shows the TTL estimations for the LPS longitudinal shift TTL noise estimation with a shifted beam waist location. The TTL noise estimations need to be under $10^{-12}\frac{m}{rtHz}$ in order to not be considered problematic for the operation of LISA. If the noise exceeds $10^{-12}\frac{m}{rtHz}$ then it would be a problem for LISA detections.

LPS Longitudinal Shift TTL Noise Estimation with Shifted Beam Waist Location			
Location Shift	Coefficient ($\frac{\frac{m}{rad^2}}{m}$)	Intercept ($\frac{m}{rad^2}$)	TTL Noise Estimation ($\frac{m}{rtHz}$)
-1.5	0.376337029	1.00054E-22	3.76337E-13
-0.75	0.376336773	1.76925E-17	3.76354E-13
0	0.376336653	-1.76923E-17	3.76319E-13
0.75	0.376336668	8.84633E-18	3.76346E-13
1.5	0.376336819	-8.84613E-18	3.76328E-13

The second table shows the TTL estimations for the LPS lateral shift TTL noise estimation with a shifted beam waist location. The TTL noise estimations need to be under $10^{-12}\frac{m}{rtHz}$ for lateral shifts as well, however, our results showed that the estimations are in the $10^{-9}\frac{m}{rtHz}$ range which is too large to be negligible. We discovered this is a mistake in the graphs, however, we did not have time to go back and fix the error making all of the lateral data negligible.

The third table shows the TTL estimations for the LPS longitudinal shifts with resized beam waists. The estimations average around $10^{-13}\frac{m}{rtHz}$ making them bellow the desired $10^{-}12\frac{m}{rtHz}$ range and therefore not worrying sources of TTL noise.

The fourth table shows the TTL estimations for the LPS lateral shifts with resized

LPS Longitudinal Shift TTL Noise Estimation with Resized Beam Waist			
Resized (%)	**Coefficient ($\frac{\frac{m}{rad^2}}{m}$)**	**Intercept ($\frac{m}{rad^2}$)**	**TTL Noise Estimation ($\frac{m}{rtHz}$)**
-10	0.360257065	1.00054E-22	3.60257E-13
-5	0.368488141	1.00008E-22	3.68488E-13
0	0.376336653	1.00131E-22	3.76337E-13
5	0.360257065	1.00131E-22	3.60257E-13
10	0.390612425	1.00087E-22	3.90612E-13

beam waists. The estimations average around $10^{-9}\frac{m}{rtHz}$ making them above the desired $10^{-12}\frac{m}{rtHz}$ range as with the other lateral set of data, for the same reasons as before, this data was discarded.

LPS Lateral Shift TTL Noise Estimation with Resized Beam Waist			
Resized (%)	**Coefficient ($\frac{\frac{m}{rad^2}}{m}$)**	**Intercept ($\frac{m}{rad^2}$)**	**TTL Noise Estimation ($\frac{m}{rtHz}$)**
-10	-0.736794921	1.38044E-16	-7.36795E-09
-5	-0.745527223	1.34843E-16	-7.45527E-09
0	-0.753514146	1.27651E-16	-7.53514E-09
5	-0.76079356	1.37373E-16	-7.60794E-09
10	-0.767415464	1.35515E-16	-7.67415E-09

Throughout the Geometric TTL Estimations portion of this project we were able to observe the Longitudinal and Lateral QPD Shifts changing the LPS and OPD. We were also able to look at how changing the measurement beam waist size and location changes LPS and OPD in some scenarios. Overall we achieved TTL estimations for the areas we looked into and found the longitudinal displacement data to be bellow the desired noise range of $10^{-12}\frac{m}{rtHz}$ around an average $10^{-13}\frac{m}{rtHz}$. However, the lateral data needs to be redone in the future because the estimations are incorrect.

5.2 Tilt-to-Length Subtraction through Time Delay Interferometry

There are no conclusive results on the TTL subtraction portion of the project because there was not enough time to finish. For this project we were able to find that foreground noise makes a difference in the TTL coefficient results as shown by the final graph (13). We were able to achieve better estimations for TTL Coefficients when adjusting frequency range from 1e-4 (Hz) to 2e-3 (Hz). If I were to continue this project I would include error bars and observe high frequency data set to look at ways of further improving the coefficient values. However, we were able to achieve closer values to the desired 2.3 (mm/rad) compared to the beginning coefficient values.

6 References

References

[1] Danzmann, Karsten, et. al. "Laser Interferometer Space Antenna." January 20, 2017.

[2] *ESA Science Technology - LISA Pathfinder*. September 13, 2021.

[3] *Gravitational Waves Detected 100 Years After Einstein's Prediction*. Caltech, 2016.

[4] *Laser Interferometer Space Antenna (LISA)*. NASA, 2021.

[5] Tröbs, M, et al. "Reducing Tilt-to-Length Coupling for the LISA Test Mass Interferometer." Classical and Quantum Gravity, vol. 35, no. 10, 2018, p. 105001., doi:10.1088/1361-6382/aab86c.

[6] Wanner, Gudrun and Karnesis, Nikolaos. “Preliminary Results on the Suppression of Sensing Cross-Talk in Lisa Pathfinder.” Journal of Physics: Conference Series, vol. 840, 2017, p. 012043., doi:10.1088/1742-6596/840/1/012043.